© Japanese Society of Electron Microscopy
Journal of Electron Microscopy 49(2): 311–321 (2000)

Full-length paper

Semiconductor Special Issue

Mechanism for secondary electron dopant contrast in the SEM

Cordelia P. Sealy, Martin R. Castell* and Peter R. Wilshaw

Department of Materials, University of Oxford, Parks Road, Oxford OX1 3PH, UK
*To whom correspondence should be addressed. E-mail: martin.castell@materials.ox.ac.uk

Abstract The growing use of secondary electron imaging in the scanning electron microscope (SEM) to map dopant distributions has stimulated an increasing interest in the mechanism that gives rise to so-called dopant contrast. In this paper a range of experimental results are used to demonstrate the wide applicability of the technique. These results are then incorporated into a model where, in particular, the effect of the surface barrier and the vacuum level are considered. It is found that the dominant contribution to the contrast mechanism is due to the three-dimensional variation of the vacuum level outside the semiconductor.

Keywords secondary electron, doping, scanning electron microscope, semiconductors, surface barrier

Received 5 July 1999, accepted 22 September 1999

Introduction

Secondary electron (SE) emission intensity is generally the preferred signal when imaging sample topography in the scanning electron microscope (SEM). With modern field emitters and high-efficiency detectors, sub-nanometre spatial resolution is now standard on high-end SEMs. However, the overwhelming use in topography applications has detracted from the sensitivity of SEs to other materials' properties, e.g. work function, stopping power and electron mean free path. In particular, differences in work function between neighbouring areas can be used to great effect when studying surface modification. SE imaging studies of diamond have shown that by decreasing the surface barrier through hydrogenation, a factor of 30 increase in SE yield can be achieved compared with an oxygen-treated surface [1]. Similar studies by Shih *et al.* [2] report SE yields up to 84 for B-doped diamond saturated with surface hydrogen. These discoveries of large changes in the SE yield have been complemented by other experiments that detect much smaller work function changes. For example, strain in SiGe heterostructures has been detected by the associated 0.1 eV raising of the valence band edge [3], and the Si (111) (7 × 7) to (1 × 1) transition has been observed using ultra-high-vacuum SE imaging [4].

Of the recent surface barrier-related work, some of the most exciting is in the field of dopant mapping in semiconductors via SE imaging. Contrast between differently doped regions in $ZnSe_{0.5}Te_{0.5}$ diodes was reported as long ago as 1972 [5], but only in the last few years has the technique really gained momentum [6–20]. This has led to some notable successes in the areas of dopant diffusion [10–12] as shown in Fig. 1, dopant mapping in devices [13,14] as shown in Fig. 2, and studies of electrical activity of dopants [12,15]. In all these studies, regions doped *n*-type appear darker than *p*-type regions. This observation has been put on a more secure footing through experiments that show that the SE emission intensity from dopant test structures is logarithmically proportional to the active dopant concentration, which holds the promise of turning dopant imaging in the SEM into a quantitative analysis tool [16]. However, for this to succeed, an understanding of the dopant contrast mechanism must be fully developed. Current understanding of the phenomenon is based on the work of Perovic *et al.* [17], Howie [18], Castell *et al.* [9,20], and Sealy [19], relating contrast to surface band structure and electron ionization energy.

When discussing surface barrier work it is important to rigorously define the concepts of work function and ionization energy. The work function of a metal is defined as the energy required to raise an electron from the Fermi energy in the interior of a crystal to a state of rest outside the surface (the vacuum level). However, this definition is only adequate for crystals with one surface termination

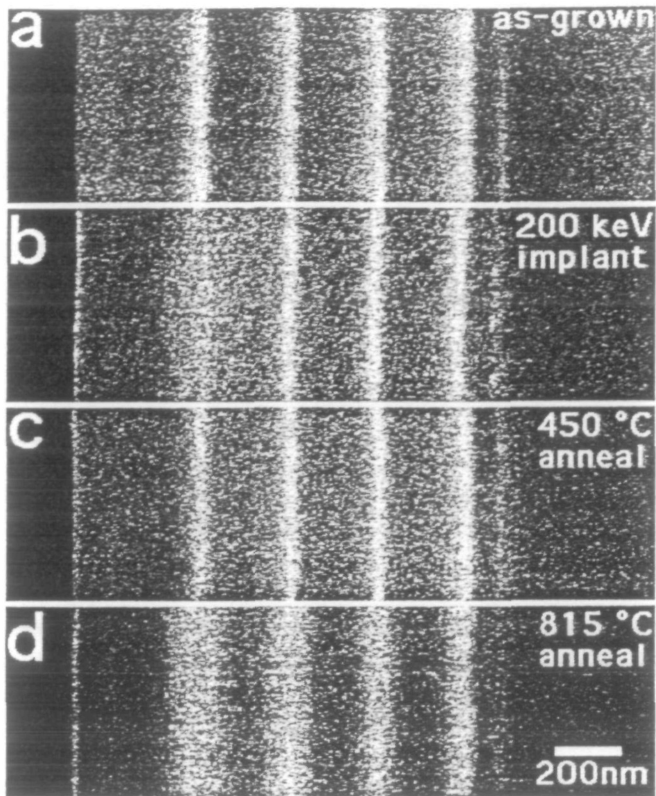

Fig. 1 Sequence of SE images of cross-sections through a Si sample containing four 25 nm B-doped layers (5×10^{19} cm^{-3}) which appear as bright vertical lines in the as-grown sample (a). After 200 keV Si ion implantation (b) the implant damage around the shallowest layer results in electrical deactivation of the B in that layer. A 450°C anneal (c) heals the damage and partially reactivates the B dopants. The broadening of the dopant peaks in (d) is due to transient enhanced diffusion following an 815°C anneal. For further details see Ref. [12].

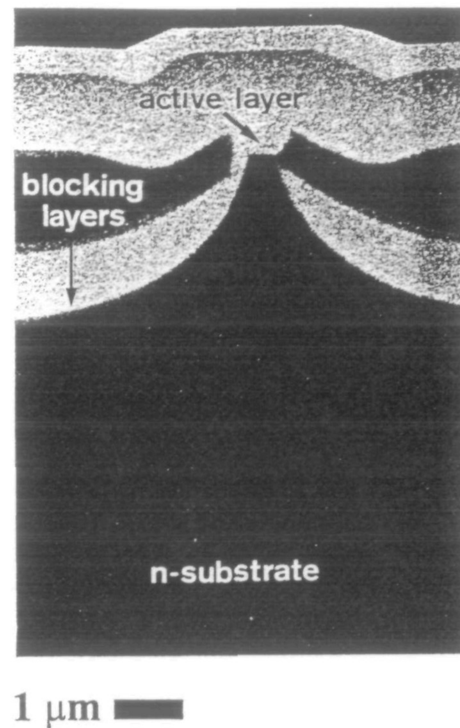

Fig. 2 SE micrograph of a laser device taken on an in-lens SEM at 2 kV. Each region of the device, the active region, blocking layers and substrate, are indicated. The device is clearly asymmetric. The poor lasing characteristics of this device can be explained by the p-type path which allows the injected current to bypass the active layer on the left hand side of the device where the blocking layers do not touch the mesa active region.

where the potential of the vacuum level just outside the surface dipole layer is equal to the vacuum level at infinity. The definition is incomplete for cases where different surface terminations are present on different faces of the same crystal because the potential of the vacuum level will then vary as a three-dimensional function outside the crystal. In such a case there are two separate and different definitions of the work function that may be used. The first is the potential energy difference between the Fermi energy and the vacuum potential just outside the surface dipole layer, i.e. in a region that is negligibly affected by the external fields. In this case surfaces with different terminations are found to have different work functions. This definition is described by Ashcroft and Mermin [21]. The second definition of work function is the energy required to take an electron from the Fermi level to a position at a macroscopic distance from the surface, and in this case is independent of the crystal face from which the electron is taken. This definition is used, e.g. by Zangwill [22]. A macroscopic distance in this context means orders of magnitude larger than the separation of the non-equivalent surface terminations on the crystal. Some definitions use 'infinity' rather than 'macroscopic distance', but these definitions are in essence equivalent.

Due to the high electron population and high density of states at the Fermi energy of a metal, substantial SE emission will occur if the SEs generated in the solid have a greater energy than the work function. For semiconductors the same statement is not true as the relatively low occupation of the conduction band and surface states means that the most relevant value for SE emission is the energy difference between the nearly fully occupied states at the valence band edge and the vacuum level. This energy is called the ionization energy. By analogy with the definitions of work function, the ionization energy can also be defined in two ways depending on whether one considers the energy required to take the electron from the top of the valence band to just outside the semiconductor (~1 nm in our case) or to a macroscopic distance (to the SE detector).

In this paper we revisit the issue of the SE dopant contrast mechanism with a quantitative treatment of the factors that change the surface barrier in n- and p-type material. In particular we find that the three-dimensional variations in the vacuum potential outside the semiconductor significantly affect the expected contrast. We

will describe how local differences in ionization energy between differently doped and undoped material give rise to contrast in the SE imaging mode of a SEM. Here we will use the definition of the ionization energy as the energy required to move an electron from the top of the valence band to a macroscopic distance from the surface of the material. The change in internal energy across a *p*–*n* junction, or any junction with different doping concentrations, will give rise to electrostatic 'patch fields' between the differently doped material due to the redistribution of charge around a *p*–*n* junction. It is these electrostatic fields, external to the material, that result in the *n*- and *p*-type material having different ionization energies, and hence give rise to SE dopant contrast in the SEM. The details of these concepts will be discussed in full in the main body of the paper.

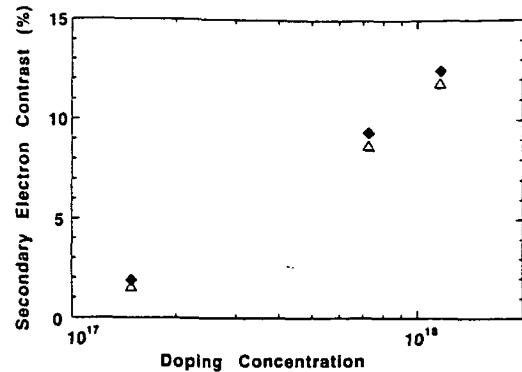

Fig. 3 Graph of SE dopant contrast as a function of Zn (*p*-type) doping concentration in InP material at 1.5 keV (filled diamonds) and 2.5 keV (open triangles).

Review of experimental results

Methods

The dopant contrast observed in a SEM is dependent on a number of parameters. These may be grouped as follows.

(1) Material properties, including semiconductor type, band gap, ionization energy, doping type and concentration.
(2) Specimen surface effects, e.g. the presence of surface states and/or contaminants and oxides which depend upon the semiconductor type, specimen preparation and the vacuum quality in the SEM.
(3) Experimental conditions that influence the collection of SEs carrying the dopant contrast signal and include working distance, detector type, accelerating voltage and beam current.

In this section a wide range of experimental results are reviewed, including those from different materials and obtained using different types of SEM. In each case, specimen preparation consisted of cleaving in air and was sometimes followed by a chemical treatment, e.g. an HF dip. Full details of the experimental methods and materials are described elsewhere [13,14,19]. Throughout the work presented here an identical experimental methodology was followed. In each case, the SE signal from the specimen was measured in the form of multiple line-scans taken directly from the SEM using a computer to collect and average the data. Initially a zero level for the SE signal was determined by blanking out the primary electron beam and recording line-scans. The beam was then restored and the SEM brightness and contrast levels were left unaltered. The zero level was subtracted from each line-scan to determine absolute signal levels. The absolute SE signal line-scans were then used to determine the contrast between *p*- and *n*-type regions of the specimen according to the relation

$$C(pn) = \{S(p) - S(n)\}/S(n)$$

where $S(p)$ and $S(n)$ are the SE signal levels from *p*- and *n*-doped material, respectively. $C(pi)$ and $C(ni)$ can be similarly defined as the contrast between *p*- or *n*- and *i*-type material. The dopant contrast values determined in this way from absolute signal levels represent true contrast values, and are independent of the contrast and brightness settings of the microscope.

Materials properties

This investigation of the sensitivity of contrast to activated *p*- and *n*-type dopant concentrations in InP, InGaAs and InGaAsP material found that *n*-type doping levels greater than $\sim 7 \times 10^{17}$ cm^{-3} and *p*-type as low as $\sim 1 \times 10^{17}$ cm^{-3} gave rise to contrast relative to intrinsic material in the SE imaging mode. Figure 3 shows the linear relation between the logarithm of doping concentration and SE contrast. Although a range of different semiconductor materials (Si, InAs, GaAs, InP) was analysed, all the specimens had different doping levels and could not be directly compared. It was not possible in the course of this work to determine the existence of any relation between contrast level and characteristic band gap.

Throughout this work it has proved very difficult to distinguish between *n*- and undoped (or *i*-type) material. A distinction between these types of doped regions is just possible in highly doped InP- and HF-treated silicon material. Similarly to Venables and Maher [10], no dopant contrast was observed to arise from the n^+ region of n^+–*p* junctions in silicon MOSFET structures. While in this case it could be due to the resolution limit of the microscope used, charging or local fields associated with polysilicon and metal layers, it could also be fundamental to the mechanism.

Specimen surface effects

After cleaving, chemical treatments can be applied to silicon and InP specimens to passivate surface states. Although cleavage-associated surface states in III–V material are traditionally assumed to be outside the band

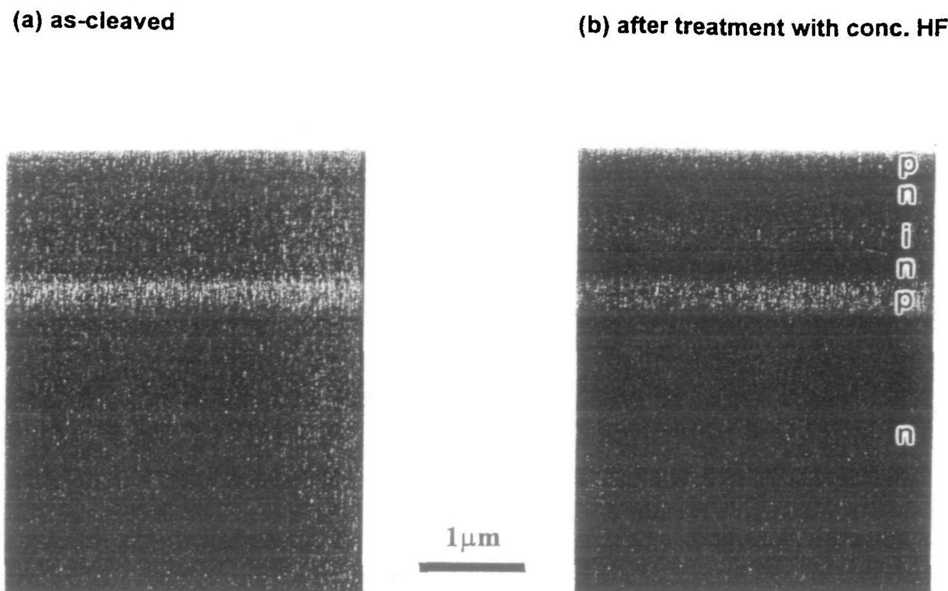

Fig. 4 SE micrographs of Si before (a) and after (b) treatment with concentrated HF taken at 2.5 keV. Only the 10^{18} cm^{-3} doped *p*-type layers are visible prior to treatment (a), compared to (b) where the 10^{18} cm^{-3} doped *n*- and *i*-type layers can be distinguished.

gap, surface-induced states will arise from adsorbates (as cleaving is performed in air). The most standard passivation treatment is a dip in HF. The treatment of silicon specimens with HF is observed to increase contrast between *n*- and *i*-type and *n*- and *p*-type regions, as shown in Fig. 4. Similar treatments performed on InP surfaces cleaved in air appeared to have no significant effect on contrast levels, except for an HF-treated low doped (1.0×10^{17} cm^{-3}) specimen. This apparently contradictory result arises from the fundamentals of the contrast mechanism and will be shown to be consistent with the proposed mechanism.

Contamination is a common problem in electron microscopy, but has been found to be particularly detrimental to the observation of contrast in this work. The presence of contamination, typically a polymerized hydrocarbon layer, has been observed to significantly reduce contrast levels. The fact that storage time in air and various chemical treatments did not reduce the apparent extent of this hydrocarbon contamination layer indicates that the microscope vacuum is the source of these hydrocarbon species. The elimination, as far as possible, of such contaminant species from a microscope is essential for reproducible quantitative analysis.

Experimental conditions

Figure 5 shows SE and back-scattered electron (BSE) images of the same sample taken under similar conditions, and unambiguously demonstrates that contrast from differently doped regions does not arise in the BSE imaging mode. This result indicates that dopant contrast is only generally carried by SEs rather than BSEs. No investigations report that BSEs exhibit doping contrast, presumably because any difference in average atomic number between *p*- and *n*-type-doped material is too small to be detected by changes in the BSE signal.

Contrast can be observed in SEM instruments with conventional detectors, but it is enhanced when using an in-lens geometry [10,19]. This is believed to be due to the preferential collection of SEs produced from the near-surface region of specimens and the suppression of the contribution from SEs produced by scattering from the lens, pole-piece and chamber walls. Contrast in an in-lens collection system microscope is also observed to increase in magnitude (and change in appearance) at shorter working distances [19].

As shown in Fig. 6, contrast levels are also found to increase at low accelerating voltages (and have the added advantage that beam breakthrough at the specimen edge is minimized). This observation can be explained by the fact that the generation volumes of both SEs that are produced by the incident beam and those that are generated when BSEs exit the sample are of the order of the dimensions of the differently doped layers under these conditions (from calculation of the Bethe range), and both will, therefore, contribute to the collected signal.

The dependence of contrast on the microscope beam current is also reported here for the first time. In all cases it was found that the magnitude of the contrast levels increased with decreasing beam current, as shown in Fig. 7. While this result does not definitively contribute towards an explanation of the contrast effect, it will be shown to be consistent with the mechanism proposed here.

As with all other techniques that rely on the electrical

(a) With SE-detector only

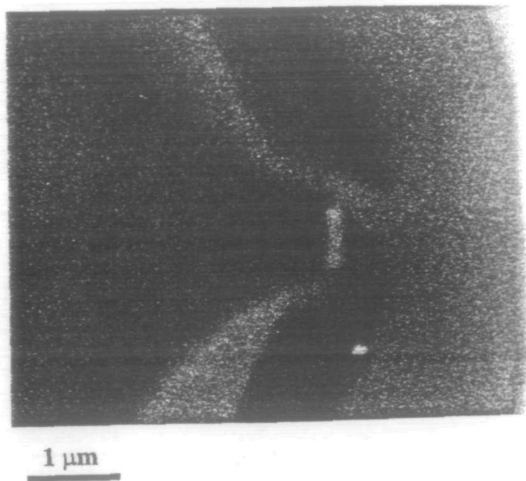

(b) With BSE-detector only

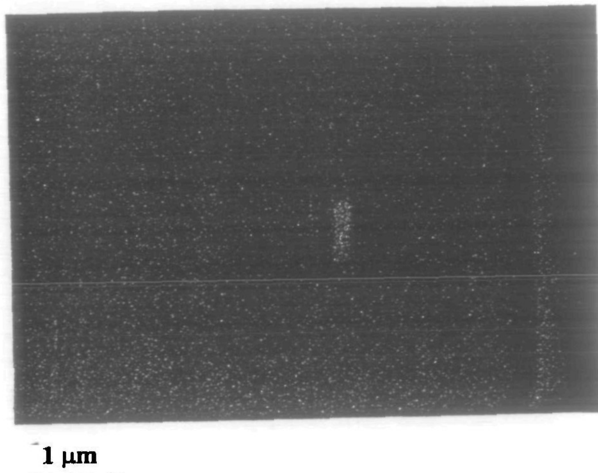

Fig. 5 SE micrographs show a cross-section through an InP/InGaAsP laser device taken on a standard SEM at 10 kV with (a) a standard Everhart–Thornley SE detector and (b) a BSE detector. Only the active region and capping layer can be seen in the BSE mode (b), whereas the SE mode also shows the *p* and *n* dopant distributions.

effect of dopants for detection, the resolution of SE imaging is limited by the Debye length. This is defined as,

$$L_D = \{\varepsilon_S(kT/e)/eN_a\}^{1/2} \qquad (1)$$

where ε_S is the permittivity of a semiconductor and N_a is the doping concentration [23]. Consequently, provided the microscope can resolve features smaller than the Debye length at the contrast levels produced by dopants, then the image resolution will be limited by the specimen rather than the microscope itself. Interestingly, as microelectronic device dimensions shrink, their doping concentrations are increased so that the Debye length in the active region is always less than the characteristic dimensions of the device. This implies that doping contrast in the SEM will continue to be able to provide information with

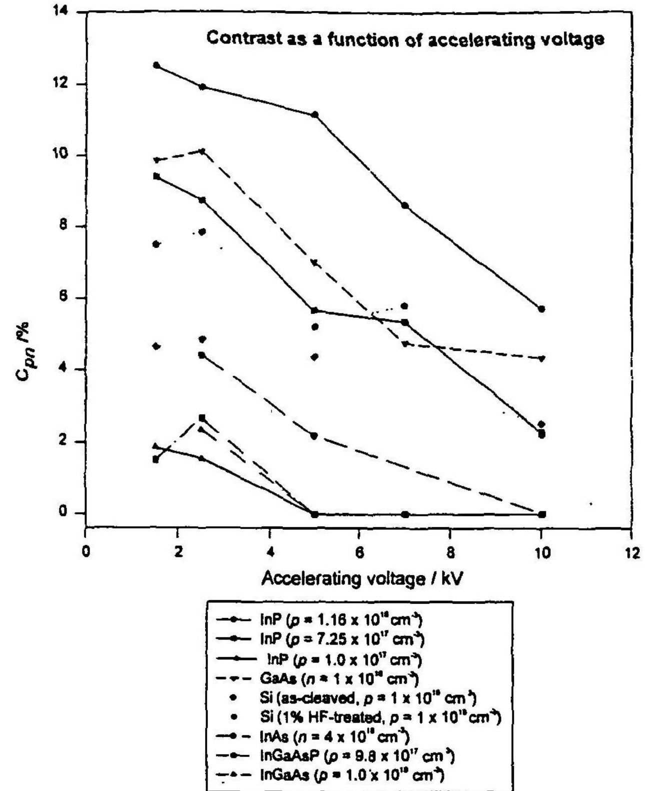

Fig. 6 The graph shows contrast levels (C_{pn}) as a function of accelerating voltage at a beam current of 6×10^{-12} A for various materials.

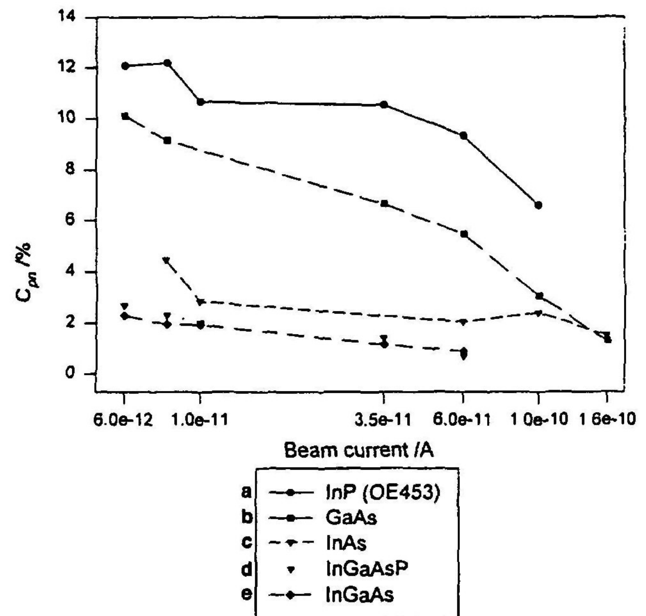

Fig. 7 Graphs show dopant contrast (C_{pn}) as a function of beam current at an accelerating voltage of 2.5 keV for various materials: (a) as-cleaved InP with *p*- and *n*-type layers doped at 1×10^{18} cm^{-3}; (b) GaAs with *p*- and *n*-type layers doped at ~ 10^{18} cm^{-3}; (c) InAs with an *n*-type layer doped at ~ 4×10^{18} cm^{-3}; (d) InGaAs with *p*-type layers doped at 3×10^{18} cm^{-3} and 1×10^{18} cm^{-3}; (e) InGaAsP with *p*-type layers doped at 9.8×10^{17} cm^{-3} and 4.8×10^{17} cm^{-3}.

sufficient resolution even as devices continue to shrink in size. For example, at a doping concentration of 10^{19} cm^{-3} the Debye length in silicon at 300 K is ~1.3 nm.

These results have demonstrated the sensitivity of dopant contrast to a wide range of factors arising from the material itself, its surface condition and the experimental conditions used. Any postulated mechanism must be able to account for the dependency of contrast on all these factors. The following discussion will describe the most comprehensive treatment of the contrast mechanism to date.

Discussion: contrast mechanism

To explain the results described, we must account for the difference in SE emission between undoped and *p*-, *n*- and *i*-doped material. The energy required for the emission of a SE originating within the bulk of a crystal not only depends upon the interior conditions but also those at the surface [21,22]. This consideration arises because the termination of the bulk crystal structure at the surface produces local distortions in the electronic charge distribution as surface ions are generally displaced slightly from their ideal lattice positions. This local distortion means that the surface of a solid possesses an electric dipole moment or even a net electrical charge. The magnitude of this effect depends on surface roughness, the orientation of the surface plane with respect to the crystallographic axes, and also the dopant type, which is considered here.

For an arbitrary metal for which all surfaces are assumed for simplicity to have equivalent structures, then far away (on the atomic scale) from the electronically neutral surface, the charge distribution of individual distorted cells at the surface produces no macroscopic field. Within the surface layer where cells are distorted, however, an electric field is appreciable and demands that an electron moving through this layer will have to perform an amount of work,

$$W_S = \int e\mathbf{E}.\, dl \qquad (2)$$

where e is the electronic charge, $\mathbf{E}$ is the electric field and l is the distance (in terms of the layer width). If this layer of surface cell charge distortion is considered to be a uniform macroscopic surface density of dipoles, it is referred to as the 'double layer'. The amount of work, W_S, necessary to move an electron through the double layer gives rise to the threshold energy required for emission.

In the case of a *p–n* junction, the crystal surface is considered to be non-uniform with respect to doping, and a net macroscopic surface charge can exist in different regions in addition to the double layer, provided that charge neutrality over the whole of the specimen is preserved. If an electron is removed from the *n*-type side of the junction into the vacuum, and then returned to the *p*-type side and then moved back into the n-type

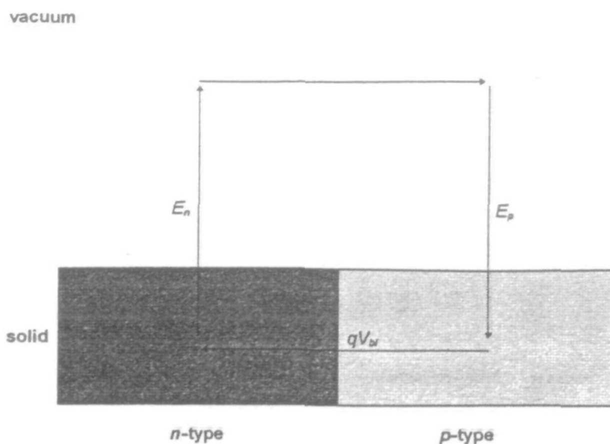

Fig. 8 A schematic representation of a *p–n* junction is shown. If an electron is moved from the interior of the *n*-type region into the vacuum and then returned to the *p*-type region, an extra amount of energy of magnitude qV_{bi} is acquired when the electron reaches its original starting point. Because the sum of the energy transitions around the closed circuit is non-zero, this situation must be corrected through the external fields in the vacuum region.

material (Fig. 8), the sum of the energy terms of this closed circuit would be non-zero if no fields existed outside the specimen:

$$E_n - E_p - qV_{bi} \neq 0 \qquad (3)$$

This assumes that $E_n = E_p$, where E_n is the energy transition out of the *n*-side, E_p is the energy transition into the *p*-side and V_{bi} is the built-in potential of the junction. However, the conservation of energy precludes this gain in energy and implies that fields must exist outside the specimen so that an extra energy term E_{BI} can be included as follows,

$$E_n + E_{BI} - E_p - qV_{bi} = 0 \qquad (4)$$

if $E_n = E_p$, then

$$E_{BI} = qV_{bi}$$

This extra energy term, E_{BI}, is then defined as the energy required to move an electron through the external fields generated by the electrostatic dipole due to the junction space charge region. Thus, for a specimen containing a *p–n* junction there must be a change in the local vacuum level outside the specimen surface due to the presence of an external field.

For the case of a *p–n* junction, the energy required to take an electron from the densely occupied valence band (E_v) to the local vacuum level (E_{vac}) (represented as transitions E_n and E_p in Fig. 9) is independent of dopant concentration (as a dopant atom represents at most 1 atom in ~50 000 bulk atoms for the materials studied in this work) and can be shown to be unaffected by band bending at the surface. Thus, the observation of contrast between *p*- and *n*-doped regions arises from the spatial variation in potential of the local vacuum level, and hence a

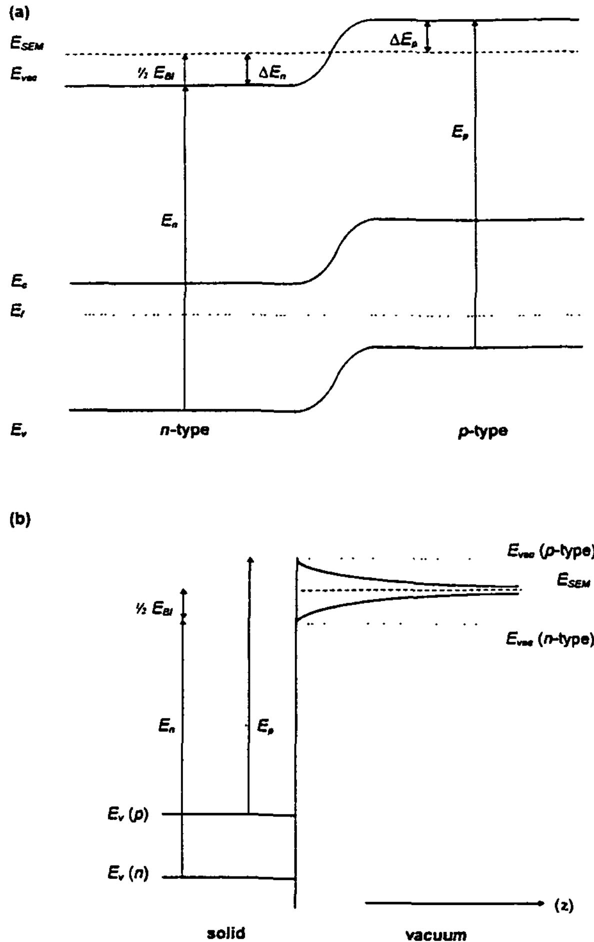

Fig. 9 (a) A schematic representation of the band structure of a p–n junction. For SE emission from p-type to E_{SEM} an amount of energy E_p is required, compared to $E_n + 1/2E_{BI}$ for n-type. This variation in energy gives rise to the collection of a different amount of SEs from each region, observed as contrast. The vacuum energy level far from the specimen surface is shown mid-way between the local levels associated with each dopant type. (b) The same schematic is shown perpendicular to the surface in terms of energy (vertical axis) and position (horizontal axis).

variation in ionization energy between n- and p-type material. This variation is produced by the built-in potential associated with the p–n junction.

The crucial factor then becomes the relative energy of an electron far from the specimen, or in this case as far as the SEM chamber walls or detector (E_{SEM}), with respect to the local vacuum level just outside the specimen. The position of E_{SEM} relative to the local vacuum level for p- and n-doped regions on either side of the junction can be determined in the following manner. From the relation for the electrostatic energy, U, in a field, ξ,

$$U = \int_v \tfrac{1}{2}\,\varepsilon_0\,\xi^2\,dV \qquad (5)$$

where ε_0 is the permittivity of a vacuum and the integration is performed over all space, the value of E_{SEM} can be found for which the electrostatic energy in the field surrounding the specimen is a minimum. The total energy associated with the electric field outside the p–n junction (assuming a large flat sheet and ignoring the effects of the material edges and lateral fields which are most significant only close to the p–n junction itself) is then,

$$U = \tfrac{1}{2}\,\varepsilon_0 \int (a_n\xi_n^2 + a_p\xi_p^2)\,dz \qquad (6)$$

where z is taken to be perpendicular to the surface, a_n and a_p are the areas of each differently doped region, ξ_n and ξ_p are the components of the fields from each region in the z-direction. It is then assumed that,

$$\xi_n(z) = \Delta E_n \cdot f(z) \qquad (7)$$

$$\xi_p(z) = -\,\Delta E_p \cdot f(z) \qquad (8)$$

where $f(z)$ is the form of the dependence of the field on distance and is identical in each case. The magnitude of the field outside of the specimen is then proportional to the difference in energy of an electron near and far from the specimen surface (ΔE_n and ΔE_p), substituting Eqs (7) and (8) into Eq. (6)

$$U = \tfrac{1}{2}\,\varepsilon_0\,[a_n\,\Delta E_n^2 \int f(z)\,dz + a_p\,\Delta E_p^2 \int f(z)\,dz]$$

$$U \propto a_n\,\Delta E_n^2 + a_p\,\Delta E_p^2 \qquad (9)$$

From Fig. 9 it can be seen that,

$$\Delta E_n + \Delta E_p = E_{BI}$$

which can be substituted into Eq. (9), to give

$$U \propto (E_{BI} - \Delta E_p)^2\,a_n + a_p\,\Delta E_p^2$$

The minimum energy in the electrostatic field outside the specimen is obtained when

$$\Delta E_p = (E_{BI}a_n)/(a_n + a_p) \qquad (10)$$

where if $a_n = a_p$ then,

$$\Delta E_p = \tfrac{1}{2}\,E_{BI}$$

and the energy of an electron far from the specimen surface lies mid-way between the vacuum level energies just outside the surfaces of the n- and p-type regions. This analysis shows that the position of the distant energy level (E_{SEM}) will lie somewhere between the local vacuum energy levels (E_{vac}) associated with each different dopant type depending upon the relative area of each region. In the following discussion of the contrast mechanism, it is assumed for simplicity that the area of each region is equal so that the distant energy level lies mid-way between the local levels. This model system is shown in Fig. 9. It should be noted that for $a_n \neq a_p$ then $\Delta E_n \neq \Delta E_p$. For example, for a small region of n-type material surrounded by a large amount of p-type material, $a_n << a_p$ and hence $\Delta E_n >> \Delta E_p$. This result predicts a lack of visibility of a small region of p-type material embedded in n-type material, but is not discussed further in this paper.

For an emitted electron to be collected it must have sufficient energy to surmount the highest energy barrier (either E_{vac} or E_{SEM}). Thus, an electron emitted from the p-type side of the junction must have sufficient energy to

reach E_{vac} (which is equal to E_p), whilst from the n-type side an extra energy component of the order of $1/2E_{BI}$ is required (in addition to E_n) to reach E_{SEM}. The lower energy necessary for SE emission from p-type material will give rise to a higher SE signal, so that it appears bright in comparison to n-type. For a material, e.g. silicon, with a band gap energy of 1.12 eV, the change in local vacuum level (E_{BI}) is likely to be of the order of ~ 1.0 eV. Thus, it can be deduced that SE emission from a region of n-type material will require an extra component of energy of the order of ~ 0.5 eV, a fairly substantial amount. This effect is also described by Howie [18]. Moreover, the value of V_{bi} and hence E_{BI} is logarithmically dependent on doping concentration [23], and this explains, in general terms, the experimentally observed logarithmic dependence of SE contrast on junction doping.

The effect of surface band bending

The abrupt termination of a periodic crystal structure at a surface after cleaving results in unsaturated atomic bonds (or dangling bonds) at the newly formed surface which induce electronic states. A semiconductor cleaved in air will usually contain surface states that are located in the band gap and can pin the Fermi level (E_f) to a near mid-gap position at the surface [24]. The surface states can trap free carriers from the bulk material resulting in a charge accumulation region at the surface and associated band bending. The presence of this band bending reduces the difference in ionization energy between n- and p-type regions (as shown in Fig. 10). At the surface, where SEs are generated, the difference in energy between the valence bands in the n- and p-type material is now reduced from qV_{bi} by the amount of the surface band bending. In the most extreme case, if the Fermi level was pinned exactly in the mid-gap position there would be no difference in the energy required for SE emission between n- and p-type material and no contrast would be observed. Thus, the surface condition of a specimen, in terms of the presence of surface states, significantly reduces the observed contrast.

Surface treatment with HF is known to remove surface native oxide layers and is also reported to passivate surface dangling bonds, and their associated states, produced during cleaving [25,26]. It was found in this work that HF treatment increased contrast between n- and i-type and n- and p-type regions in silicon specimens. The removal of native oxide alone cannot explain why HF treatment should allow a previously invisible layer (nominally undoped or i-type) to be distinguished. However, passivation of surface states in the model system shown in Fig. 10 can explain the observed behaviour. In general a given density of surface states will produce more surface band bending in lightly doped than heavily doped specimens. In heavily doped specimens the high concentration of charge carriers is more easily able to compensate for the charge due to occupied surface states. Moreover, a

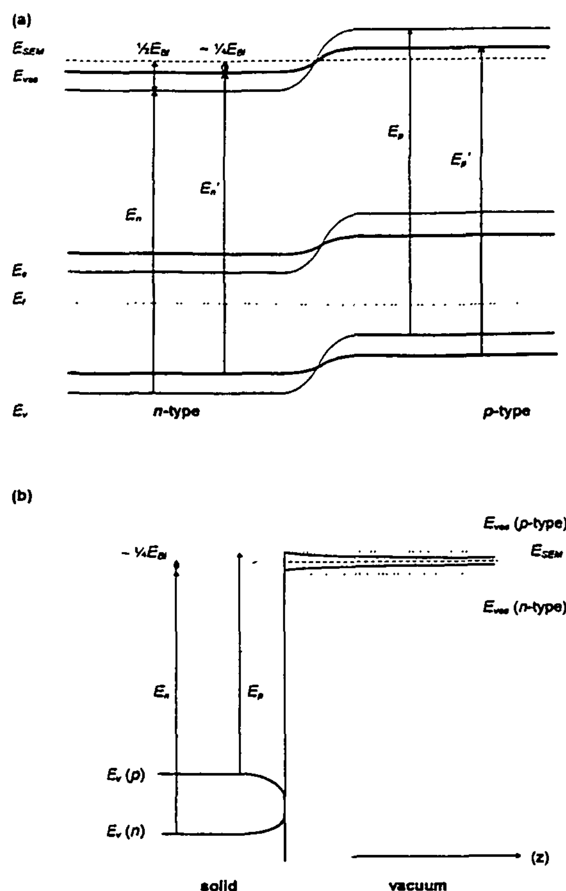

Fig. 10 A schematic representation of the band structure of a p–n junction, with the energy transitions necessary for SE emission from each side of the junction shown as before, but the new energy level positions as a result of band bending due to surface states are shown in bold. The diagram is drawn to represent the case where surface band bending reduces the contrast by approximately half.

reduction in the density of surface states due to a passivation treatment will thus have a greater effect on lightly doped than heavily doped specimens. This effect was observed experimentally and was also noticeable in the case of n-type silicon for which the surface band bending induced by surface states was sufficient to pin the Fermi level so close to the middle of the gap that no contrast between n- and i-type material was observed. However, when a surface passivation treatment was carried out to reduce the effect of surface band bending the contrast was then significant.

HF is not generally regarded as a method of passivation for Group III–V surfaces and would not be expected to have an effect on contrast levels, as observed. However, the fact that some enhancement in contrast levels on a low doped (1.0×10^{17} cm^{-3}) InP specimen was found indicates that some passivation of surface states did occur. As suggested above, a change in surface state density is likely to have a more noticeable effect at low doping concentrations near the limit of sensitivity. At the opposite extreme, a change in the density of surface states in a

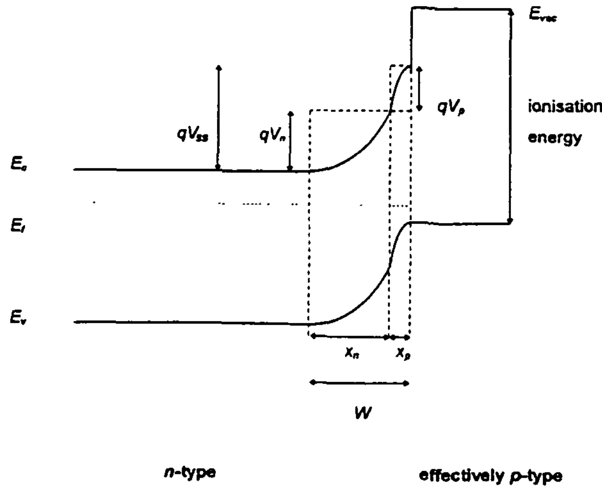

Fig. 11 The case at a solid surface where band bending due to the presence of surface states is shown schematically. This is analogous to an asymmetric p–n junction where N_A does not equal N_D. The total built-in potential due to surface states (qV_{SS}) and the depletion region (W) are defined. The term qV_n represents the band bending produced by the surface states, whilst qV_p is the energy additional to the ionization energy required for an electron to move through the surface dipole layer into the vacuum.

high doped material will make little difference to the observed contrast level.

It has been suggested that the charge trapped in the surface states is itself a contributor to the dopant contrast effect [9,17,18,20]. An estimate of the additional energy required to move an electron through this surface dipole due to the charge in the surface states can be made in the following manner to investigate the extent of its effect on the contrast. The surface charge contained in the occupied surface states is of the opposite sign to that contained in the subsurface depletion region which accounts for the majority of the surface band bending. The spatial distribution of one polarity charge in the surface space charge region and the other polarity charge in the surface states is analogous to the charge distribution in a p–n junction which has different doping concentrations on either side of the junction ($N_A \neq N_D$). In the surface case considered here, N_D is the actual doping concentration in the bulk material and N_A is an effective concentration such that $N_A x_p$ is equal to the total charge trapped in the surface states and x_p is the thickness of the surface layer over which the charge in the surface states is distributed. The situation for an n-type specimen is shown in Fig. 11. Charge neutrality demands equal amounts of charge in the surface depletion region and in the surface states themselves. The built-in potential due to the occupied surface states (V_{SS}) is the sum of the contribution due to the bent bands as they approach the surface V_n and the potential across the occupied states themselves V_p.

$$V_{SS} = V_n + V_p \tag{11}$$

Then, Poisson's equation can be used to derive a relation for the depletion region width, W, in terms of the built-in potential (V_{SS}):

$$W = \sqrt{(2\varepsilon_S V_{SS}/qN_B)} \tag{12}$$

where the doping concentration $N_B = (N_A + N_D)/N_A N_D$ and ε_S is the permittivity of the semiconductor. The contributions from the bent bands and surface charge to the built-in potential, V_{SS}, are defined as

$$V_n = \tfrac{1}{2}\,\xi_m\,(x_n) \tag{13}$$

$$V_p = \tfrac{1}{2}\,\xi_m\,(x_p) \tag{14}$$

where ξ_m is the maximum electric field [23]. Then, dividing Eq. (13) by Eq. (14) gives,

$$V_n/V_p = x_n/x_p$$

or

$$V_n/x_n = V_p/x_p \tag{15}$$

Thus, qV_p represents the extra component of energy required for SE emission due to the surface dipole and x_p is the width of this surface charge layer. For a material, e.g. silicon, with a doping concentration of ~10^{18} cm^{-3}, the depletion region width, x_n, is ~ 300 Å, and x_p, the thickness of the surface charge layer, is estimated to be of the order of the size of the unit cell, ~5 Å. From Eq. (15),

$$V_n/300 = V_p/5$$

so

$$V_n = 60V_p$$

substituting into Eq. (12), where $\varepsilon_S/\varepsilon_0 = 11.9$ (dielectric constant), $N_B \approx 10^{18}$ cm^{-3},

$$V_n \approx V_{SS} \approx W^2 qN_B/2\varepsilon_S \approx 1.0 \text{ V}$$

and from Eq. (11),

$$V_p \approx 0.02 \text{ V}$$

This is the extra energy required for SE emission from n-type material with a surface dipole. For a p-type specimen the effect of a surface dipole would be to reduce the energy required for SE emission by this amount. Suggestions that the surface dipole contributes to the observed contrast [9,17,18,20] are not borne out by this calculation which shows that its effect on the energy transitions for SE emission from p- and n-doped regions is negligible. It should be pointed out that the bent band diagrams in Refs [9,17,18,20] differ from that in Fig. 10b because the surface state dipole was thought to be significant at that time.

The doping concentration sensitivity limit of the contrast is fundamental to the effect itself and again related to band bending. If zero contrast is exhibited by a p–n junction with doping concentrations of $<5 \times 10^{16}$ cm^{-3}, it is implied that the density of surface states and the associated band bending is sufficient to pin the Fermi level, E_f, in a mid-gap position. This situation dictates that

the ionization energy is identical for both materials so that no contrast can arise. An approximate estimation of the requisite density of surface states for a mid-gap Fermi level at the sensitivity limit (5×10^{16} cm^{-3}) can be obtained as follows. The amount of band bending for *p*-type material doped at 5×10^{16} cm^{-3} is

$$E_g/2 - (E_f - E_v) \tag{16}$$

but

$$(E_f - E_v) = kT \ln (N_v/N_A) \tag{17}$$

where N_v is the effective density of states in the valence band and is 1.04×10^{19} cm^{-2} for silicon (at 300 K). The amount of band bending, by analogy with a *p–n* junction (from Eq. (11)), is defined as,

$$V_p = \frac{1}{2} q N_A x_p / \varepsilon_S \tag{18}$$

and can be used to determine the extent of the band bending as,

$$x_p = \sqrt{(2V_p \varepsilon_S / N_A q)}$$

The concentration of occupied surface states must then be the product of the extent of band bending and the doping concentration,

$$x_n \cdot N_A = \sqrt{(2V_p \varepsilon_S N_A / q)}$$

and substituting V_p in terms of the amount of band bending (from Eqs (16) and (17)) as follows,

$$V_p = q\{E_g/2 - (E_f - E_v)\}$$

determines the concentration of occupied surface states necessary to pin E_f mid-gap in this case as:

$$5.25 \times 10^{11} \text{ cm}^{-2}$$

This calculated value for the concentration of occupied surface states is well within the range quoted in the literature for the density of surface states for silicon ($\sim 10^{11} - 10^{13}$ cm^{-2}). Thus, at a doping concentration of 5×10^{16} cm^{-3} a typical density of surface states can easily pin the Fermi level mid-gap, rendering the difference in ionization energy between *p*- and *n*-type zero so that no contrast is observed. However, doping concentrations greater than this can compensate for the effect of surface states and enable contrast to be observed. This can account for the observed sensitivity limit of $>5 \times 10^{16}$ cm^{-3}, although V_{bi} (the built-in potential across a *p–n* junction in bulk material) is still fairly large at these values [23] and indicates that sensitivity might be improved further if the density of surface states could be reduced.

The beam current can also be expected to alter band bending. It has been observed that contrast increases with decreasing beam current. There are three possible explanations that will be outlined here and compared to the model of the contrast mechanism.

(1) Firstly, it is possible that as the beam current is increased the surface band bending is decreased until a flat-band condition is approached. This is due to the capture of beam-induced minority carriers in the surface potential well produced by the bent bands. The charge on the trapped minority carriers will tend to compensate for the trapped surface charge and hence reduce the band bending. A reduction in surface band bending would imply that the contrast level should increase, but this is not observed experimentally.

(2) Secondly, it is known that the high-energy incident beam produces electron-hole pairs in a region below the specimen surface defined as the generation volume. If the concentration of carriers generated in this way exceeds the doping concentration, then this region could appear to be effectively intrinsic. In this situation, it might be expected that contrast between *p*- and *n*-type regions might be lost. A simple approximation of this effect [19] has shown that the injected carrier concentration is much less than the doping concentration and will not affect the observed contrast determined, as it is, by the doping concentrations on either side of a *p–n* junction.

(3) The electron beam-induced voltage is expected to reduce the built-in bias of the junction, which could account for the reduced contrast levels at higher beam currents. The value of the electron beam-induced voltage depends logarithmically on beam current and is larger for *p–n* junctions with small cross-sectional areas and small reverse bias leakage currents. Thus, the magnitude of this effect will depend on the details of the specimen junction and not simply on the doping levels of the material from which it is comprised. It is this effect which is thought to account for the experimentally observed dependence of contrast on beam current.

Concluding remarks

We have shown that the contrast mechanism exhibited in the SE imaging mode between differently doped regions arises predominantly from the difference in energy required for electron emission from these regions and would be better called 'ionization energy contrast'. The contrast observed between differently doped regions is just one example of this effect.

The surface condition of a specimen has been demonstrated to be a fundamental limitation on sensitivity and reproducibility for this technique. The control and minimization of this factor may turn out to be the crucial factor in allowing this technique to be widely adopted for dopant mapping. However, many questions still remain unanswered, and conclusive verification of the current hypotheses regarding the mechanism that produces this phenomenon is yet to be shown.

SE imaging appears to have great potential if it can be shown to produce dopant profiles routinely. In-lens

specimen position FE-SEMs can now resolve features at the nanometre scale. These capabilities compare very well to other novel techniques, e.g. those based on probe microscopy methods. The advantage of SE imaging lies in its immediate generation of useful two-dimensional dopant information without complex sample preparation or subsequent analysis. Qualitative dopant distribution maps can give an indication of dopant type, location and concentration, but do require calibration to produce meaningful quantitative information.

References

1 Malta D P, Posthill J B, Humphreys T P, Thomas R E, Fountain G G, Rudder R A, Hudson G C, Mantini M J, and Markunas R J (1994) Secondary electron emission enhancement and defect contrast from diamond following exposure to atomic hydrogen. *Appl. Phys. Lett.* **64:** 1929–1931.

2 Shih A, Yater J, Pehrsson P, Butler J, Hor C, and Abrams R (1997) Secondary electron emission from diamond surfaces. *J. Appl. Phys.* **82:** 1860–1867.

3 Castell M R, Perovic D D, and Lafontaine H (1997) Electronic contribution to secondary electron compositional contrast in the scanning electron microscope. *Ultramicroscopy* **69:** 279–287.

4 Homma Y, Suzuki M, and Tomita M (1993) Atomic configuration dependent secondary electron emission from reconstructed silicon surfaces. *Appl. Phys. Lett.* **62:** 3276–3278.

5 Aven M, Devine J Z, Bolon R B, and Ludwig G W (1972) Scanning electron microscopy and cathodoluminescense of $ZnSe_xTe_{1-x}$ p-n junctions. *J. Appl. Phys.* **43:** 4136–4142.

6 Farrow R C, Maher D M, Ellington M B, Katz A, and Weir B E (1991) Interfaces in InP based optoelectronic structures: high resolution SEM. *Scanning* **13** (Suppl 1): I-45–I-46.

7 Takahashi Y, Yabuuchi Y, Inazato S, Ogura K, and Ono A (1993) Scanning electron microscope observation of As^+-ion-implanted region. *Jpn. J. Appl. Phys.* **32:** L1477–L1479.

8 Perovic D D, Castell M R, Howie A, Lavoie C, Tiedje T, and Cole J S (1994) Doping layer imaging in a field-emission scanning electron microscope. *ICEM 13-PARIS* 91–92.

9 Castell M R, Perovic D D, Richie D A, Lavoie C, and Tiedje T (1995) Topographical, compositional, and dopant contrast from cleavage surfaces of GaAs-$Al_xGa_{1-x}As$ superlattices. *Inst. Phys. Conf. Ser.* **146:** 281–284.

10 Venables D and Maher D M (1996) Quantitative two-dimensional dopant profiles obtained directly from secondary electron images. *J. Vac. Sci. Technol.* **B14:** 421–425.

11 Venables D, Jain H, and Collins D C (1998) Secondary electron imaging as a two-dimensional dopant profiling technique: review and update. *J. Vac. Sci. Technol.* **B16:** 362–366.

12 Castell M R, Simpson T W, Mitchell I V, Perovic D D, and Baribeau J-M (1999) Deactivation and diffusion of boron in ion-implanted silicon studied by secondary electron imaging. *Appl. Phys. Lett.* **74:** 2304–2306.

13 Sealy C P, Castell M R, Wilkinson A J and Wilshaw P R (1995) SEM imaging of contrast arising from different doping concentrations in semiconductors. *Inst. Phys. Conf. Ser.* **146:** 609–612.

14 Sealy C P, Castell M R, Reynolds C L and Wilshaw P R (1997) Application of secondary electron dopant contrast imaging to InP/InGaAsP laser structures. *Inst. Phys. Conf. Ser.* **157:** 561–564.

15 Turan R, Perovic D D and Houghton D C (1996) Mapping electrically active dopant profiles by field-emission scanning electron microscopy. *Appl. Phys. Lett.* **69:** 1593–1595.

16 Perovic D D, Turan R, and Castell M R (1998) Quantitive imaging of semiconductor doping distributions using a scanning electron microscope. In: *The Electron*, pp. 258–265 (IOM Communications, London).

17 Perovic D D, Castell M R, Howie A, Lavoie C, Tiedje T, and Cole J S (1995) Field-emission SEM imaging of compositional and doping layer semiconductor superlattices. *Ultramicroscopy* **58:** 104–113.

18 Howie, A (1995) Recent developments in secondary electron imaging. *J. Micros.* **180:** 192–203.

19 Sealy C P (1997) DPhil thesis, University of Oxford.

20 Castell M R (1995) PhD thesis, University of Cambridge.

21 Ashcroft N W and Mermin N D (1976) *Solid State Physics* (Saunders College Publishing, Philadelphia, USA).

22 Zangwill A (1988) *Physics at Surfaces* (Cambridge University Press, Cambridge, UK).

23 Sze S M (1981) *Physics of Semiconductor Devices* (Wiley, New York).

24 Bardeen J (1947) Surface states and rectification at a metal semiconductor contact. *Phys. Rev.* **71:** 717–727.

25 Burrows V A, Chabal Y J, Higashi G S, Raghavachari K, and Christman S B (1988) Infrared spectroscopy of Si(111) surfaces after HF treatment: hydrogen termination and surface morphology. *Appl. Phys. Lett.* **53:** 998–1000.

26 Takahagi T, Nagai I, Ishtani A, Kuroda H, and Nagasawa Y (1988) The formation of hydrogen passivated silicon single-crystal surfaces using ultraviolet cleaning and HF etching. *J. Appl. Phys.* **64:** 3516–3521.